IJournals: International Journal of Software & Hardware Research in Engineering
ISSN-2347-4890
Volume 3 Issue 6 June, 2015

Fuel Cell System using High Step-up converter with Voltage Multiplier Module

MANISH KUMAR SAHU1; NEELESH KUMAR2;
M. Tech in EEE[1]; Assistant prof.[2]

manishkumarsahu22@gmail.com[1]; neelesh.patel27@gmail.com

ABSTRACT

A novel high step-up converter is proposed for a front end Solar PV System using Fuel cell. Since a voltage-multiplier unit with an interleaved converter with higher step up characteristics asymmetrically finds a large step-up gain without operating at an critical duty cycle. The proposed Voltage-Multiplier unit consists of a conventional boost converter and inductors coupled together. However a traditional DC-DC (Boost) converter is integrated into the first phase to achieve a considerably higher voltage-conversion-ratio. The 2 phase arrangement decreases the current stress through each power based switch, as well as it constrains the input-current-ripple factors, that reduces losses due to conduction of metal–oxide–semiconductor field-effect-transistors. Again the adopted scheme operates as an active electronic clamp-circuit, that creates high voltage changes over the Switches. Hence the MOSFETs with low voltage rating may be adopted for reductions of losses due to conduction and price. The Efficiency factor betters as the amount of stored energy in leakage inductances is recycled to the output end. In a summary our proposed work represents, a circuit with an input voltage 40-V, output voltage of 380-V with output power of 1000- W operating to verify its result for analysis. However the maximum efficiency is found to be 96.8%, which shows a greater performance for our proposed technique.

Keywords: Boost–Fly-back Converter, High Step-Up, Fuel Cell Stack System, Voltage Multiplier Module.

I. INTRODUCTION

Renewable sources of energy are increasingly valued worldwide because of energy shortage and environmental contamination. Renewable energy systems generate low voltage output; thus, high step-up dc/dc converters are widely employed in many renewable energy applications, including fuel cells, wind power, and photovoltaic systems [1]–[8].The solar cell is the elementary building block of the photovoltaic technology. Solar cells are mainly composed of materials like Germanium, Silicon and Gallium Arsenide, which comes under semiconductor categories. The major behavior of semiconductors that makes them most useful is that their conductivity may easily be modified by introducing impurities into their crystal structure. Similarly the pentavalent impurities like phosphorus contains with 5 valence electrons (n-donor), donate weakly bound valence electrons to the Si, forming more –ve charge carriers in the atom.

Fuel Cells

Fuel cells (FC) are electrochemical devices that generate electricity and heat using H2 or H2-rich fuels, together with oxygen from air. They consist of an electrolyte sandwiched between two electrodes – an anode and a cathode (FC stack). Activated by a catalyst on the anode side, H2 atoms split into electrons and ions. Electrons migrate to the cathode through an external circuit and generate electricity, while ions migrate through the electrolyte and reunite with electrons and O2 on the cathode side, producing heat and water. There are variants of this basic process, depending on FC types and fuels. H2-powered FC maximize the benefits of using H2 as an energy carrier (e.g., efficiency, emission reduction), but most FC can run on other fuels. Polymer electrolyte membrane FC (PEMFC) are suitable for either vehicles or power generation. They use a solid polymer membrane electrolyte and carbon electrodes, with platinum (Pt) as a catalyst.

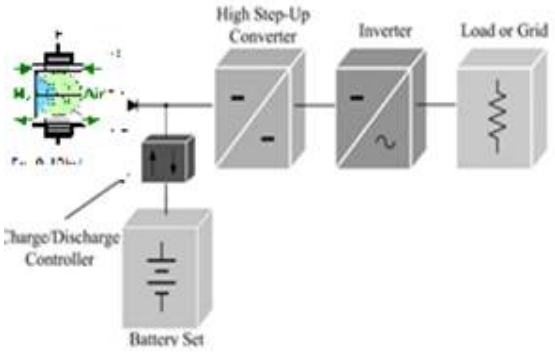

Fig.1. A typical photovoltaic system that consists of a solar module and a high step up converter.

1.1 Fuel cell concept

PEMFC are the best candidates for powering FCV as they operate at low temperature (80°C), offer short start-up time, high efficiency and good power density. An optimum power density thus exists that minimizes the energy cost, depending on the cost of H2 and the FC. The lifetime of FC needs to be improved.

The current study also presents an asymmetrical interleaved converter for a high step-up and high-power application. Modifying a boost–fly-back converter, shown in Fig. 2.2(a), is one of the simple approaches to achieving high step-up gain; this gain is realized via a coupled inductor. The performance of the converter is similar to an active-clamped fly-back converter; thus, the leakage energy is recovered to the output terminal. An interleaved boost converter with a voltage-lift capacitor shown in Fig. 2.2(b) is highly similar to the conventional interleaved type.

It obtains extra voltage gain through the voltage-lift capacitor, and reduces the input current ripple, which is suitable for power factor correction (PFC) and high-power applications. In this paper, an asymmetrical interleaved high step-up converter that combines the advantages of the aforementioned converters is proposed, which combined the advantages of both.

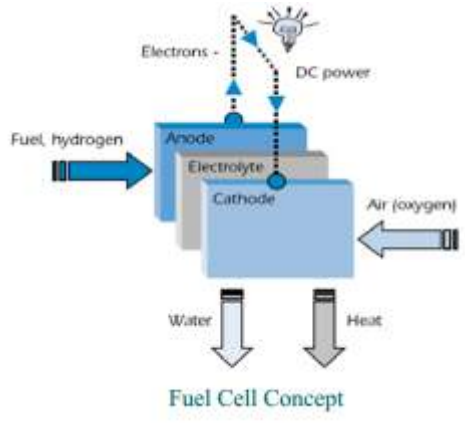

Fig. 2.1 Fuel Cell Concept

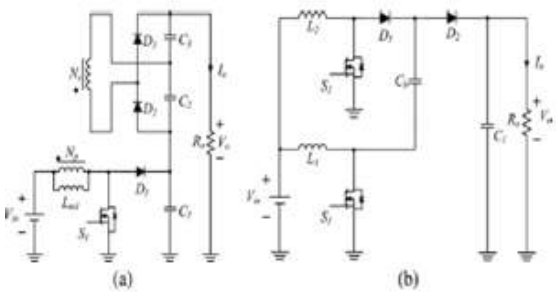

Fig. 2.2 High step-up techniques based on a classical boost converter. (a) Integrated fly-back–boost converter structure. (b) Interleaved boost converter with a voltage-lift capacitor structure.

In the voltage multiplier module of the proposed converter, the turn's ratio of coupled inductors can be designed to extend voltage gain, and a voltage-lift capacitor offers an extra voltage conversion ratio.

The advantages of the proposed converter are as follows:

1. The converter is characterized by a low input current ripple 0and low conduction losses, making it suitable for high power applications.
2. Leakage energy is recycled and sent to the output terminal, and alleviates large voltage spikes on the main switch.
3. The converter achieves the high step-up voltage gain that renewable energy systems require;
4. Low cost and high efficiency are achieved by the low *rDS* (on) and low voltage rating of the power switching device.

5. The main switch voltage stress of the converter is substantially lower than that of the output voltage.

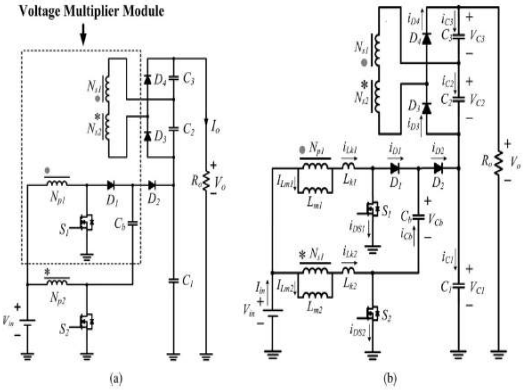

Fig.3(a). Proposed high step-up converter with a voltage multiplier module. (b).Equivalent circuit of the proposed converter.

II. OPERATING PRINCIPLE DESCRIPTION

The proposed high step-up converter with voltage multiplier module is shown in Fig. 3(a). A conventional boost converter and two coupled inductors are located in the voltage multiplier module, which is stacked on a boost converter to form an asymmetrical interleaved structure. Primary windings of the coupled inductors with *Np* turns are employed to decrease input current ripple, and secondary windings of the coupled inductors with *Ns* turns are connected in series to extend voltage gain. The turns ratios of the coupled inductors are the same. The coupling references of the inductors are denoted by "." and "*" in Fig. 3. The equivalent circuit of the proposed converter is shown in Fig. 3(b), where *Lm*1 and *Lm*2 are the magnetizing inductors, *Lk*1 and *Lk*2 represent the leakage inductors, *S*1 and *S*2 denote the power switches, *Cb* is the voltage-lift capacitor, and *n* is defined as a turns ratio *Ns*/*Np*. The proposed converter operates in continuous conduction mode (CCM), and the duty cycles of the power switches during steady operation are inter leaved with a 180◦ phase shift; the duty cycles are greater than 0.5. The key steady waveforms in one switching period of the proposed converter contain six modes, which are depicted in Fig. 4, and Fig. 5 shows the topological stages of the circuit.

Mode 1 [t0, t1]: At *t*=*t*0, the power switches *S*1 and *S*2 are both turned ON. All of the diodes are reversed-biased. Magnetizing inductors *Lm*1 and *Lm*2 as well as leakage inductors *Lk*1 and *Lk*2 are linearly charged by the input voltage source *V*in.

Mode 2 [t1, t2]: At *t*=*t*1, the power switch *S*2 is switched OFF, thereby turning ON diodes *D*2 and *D*4. The energy that magnetizing inductor *Lm*2 has stored is transferred to the secondary side charging the output filter capacitor *C*3. The input voltage source, magnetizing inductor *Lm*2, leakage inductor *Lk*2, and voltage-lift capacitor *Cb* release energy to the output filter capacitor *C*1 via diode *D*2, thereby extending the voltage on *C*1.

Mode 3 [t2, t3]*:* At *t*=*t*2, diode *D*2 automatically switches OFF because the total energy of leakage inductor *Lk*2 has been completely released to the output filter capacitor *C*1. Magnetizing inductor*Lm*2 transfers energy to the secondary side charging the output filter capacitor *C*3 via diode *D*4 until *t*3.

Mode 4 [t3, t4]*:* At *t*=*t*3, the power switch *S*2 is switched ON and all the diodes are turned OFF. The operating states of modes 1 and 4 are similar.

Mode 5 [t4, t5]*:* At *t*=*t*4, the power switch *S*1 is switched OFF, which turns ON diodes *D*1 and *D*3. The energy stored in magnetizing inductor *Lm*1 is transferred to the secondary side charging the output filter capacitor *C*2. The input voltage source and magnetizing inductor *Lm*1 release energy to voltage-lift capacitor *Cb* via diode *D*1, which stores extra energy in *Cb*.

Mode 6 [t5, t0]*:* At *t*=*t*5, diode *D*1 is automatically turned OFF because the total energy of leakage inductor *Lk*1 has been completely released to voltage-lift capacitor *Cb*. Magnetizing inductor *Lm*1 transfers energy to the secondary side charging the output filter capacitor *C*2 via diode *D*3 until *t*0.

III. STEADY-STATE ANALYSIS

The transient characteristics of circuitry are disregarded to simplify the circuit performance analysis of the proposed converter in CCM, and some formulated assumptions are as follows:

1. All of the components in the proposed converter are ideal;
2. Leakage inductors *Lk*1 and *Lk*2 are neglected;
3. Voltage *VCb*, *VC*1, *VC*2, and *VC*3 are considered to be constant because of infinitely large capacitance.

A. Voltage Gain

The first-phase converter can be regarded as a conventional boost converter; thus, voltage *VCb* can be derived from

$$V_{Cb} = \frac{1}{1-D} V_{\text{in}}. \quad (1)$$

When switch *S*1 is turned ON and switch *S*2 is turned OFF, voltage *VC*1 can be derived from

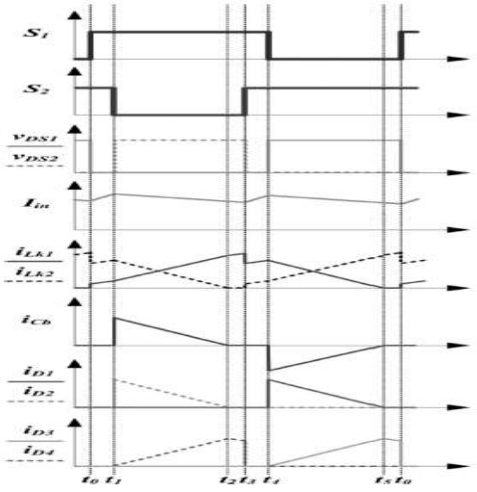

Fig. 4. Steady waveforms of the proposed converter at CCM.

$$V_{C1} = \frac{1}{1-D} V_{\text{in}} + V_{Cb} = \frac{2}{1-D} V_{\text{in}} \quad (2)$$

The output filter capacitors *C*2 and *C*3 are charged by energy transformation from the primary side. When *S*2 is in turn-on state and *S*1 is in turn-off state, *VC*2 is equal to induced voltage of *Ns*1 plus induced voltage of *Ns*2, and when *S*1 is in turn-on state and *S*2 is in turn-off state, *VC*3 is also equal to induced voltage of *Ns*1 plus induced voltage of *Ns*2. Thus, voltages and can be derived from

$$V_{C2} = V_{C3} = n \cdot V_{\text{in}} \left(1 + \frac{D}{1-D}\right) = \frac{n}{1-D} V_{\text{in}} \quad (3)$$

The output voltage can be derived from

$$V_o = V_{C1} + V_{C2} + V_{C3} = \frac{2n+2}{1-D} V_{\text{in}} \quad (4)$$

The voltage-gain is given by

$$\frac{V_o}{V_{\text{in}}} = \frac{2n+2}{1-D} \quad (5)$$

Equation (5) confirms that the proposed converter has a high step-up voltage gain without a critical duty-cycle. The characteristics for the voltage-gain shows turns ratio *n* and duty cycle is displayed in Figure no6.While the duty-cycle is assumed to be equal to 0.6, and the voltage-gain may become 10 for a turns-ratio of *n:* 1; the voltage gain reaches 30 at a turns ratio *n* of 5.

B. Voltage Stresses on Semiconductor Components

The voltage ripples on the capacitors are ignored to simplify the voltage stress analyses of the components of the proposed converter. The voltage stresses on power switches *S*1 and *S*2 are derived from

$$V_{S1} = V_{S2} = \frac{1}{1-D} V_{\text{in}} \quad (6)$$

The stressed Voltages over *S*1,*S*2 are related to the output voltage *Vo* and the turns ratio *n* can be expressed as

$$V_{S1} = V_{S2} = V_o - \frac{2n+1}{1-D} V_{\text{in}} \quad (7)$$

Equations (6) and (7) confirm that low-voltage-rated metal– oxide–semiconductor field-effect transistors (MOSFETs) with low *RDS*−ON can be adopted for the proposed converter to reduce losses due to conduction and price. All this characteristics shows our proposed technique is better for high step-up and stresses on the power switches account for half of output voltage *Vo*, even if turns ratio *n* is 0. The voltage stress on diode *D*1= *VC*1,also the stressed voltage for *D*2=*VC*1-min(*VCb)*.

Hence the stressed voltage can be given by

$$V_{D1} = V_{C1} = \frac{2}{1-D} V_{\text{in}} \quad (8)$$

$$V_{D2} = V_{C1} - V_{Cb} = \frac{1}{1-D} V_{\text{in}} \quad (9)$$

The Stressed-Voltages due to*D*1,*D*2 to the output voltage *Vo* and the turns ratio *n* can be expressed as

$$V_{D1} = V_o - \frac{2n}{1-D} V_{\text{in}} \quad (10)$$

$$V_{D2} = V_o - \frac{2n+1}{1-D} V_{\text{in}} \quad (11)$$

The voltage stresses on diodes *D*1 and *D*2 are close on power *S*1,*S*2. Since the stressed Voltage over D1 is greater, the voltage is only 50% of the voltage *Vo* at a turn-ratio of *n:* 1. The stressed voltage across the diodes are smaller as the voltage gain is extended by increasing turns ratio *n*. The voltage stresses on diodes*D*3 and*D*4 both equal the *VC*2 +*VC*3,given by

$$V_{D3} = V_{D4} = \frac{2n}{1-D} V_{\text{in}} \quad (12)$$

The stressed voltage across *D*3 ,D4 to the output voltage *Vo* and the turns ratio *n* can be expressed as

$$V_{D3} = V_{D4} = V_o - \frac{2}{1-D} V_{\text{in}} \quad (13)$$

C. Analysis of Conduction Losses

Some conduction losses are caused by resistances of semiconductor components and coupled-inductor. Hence the overall elements in the presented converter are not considered to be perfect besides the condensers.

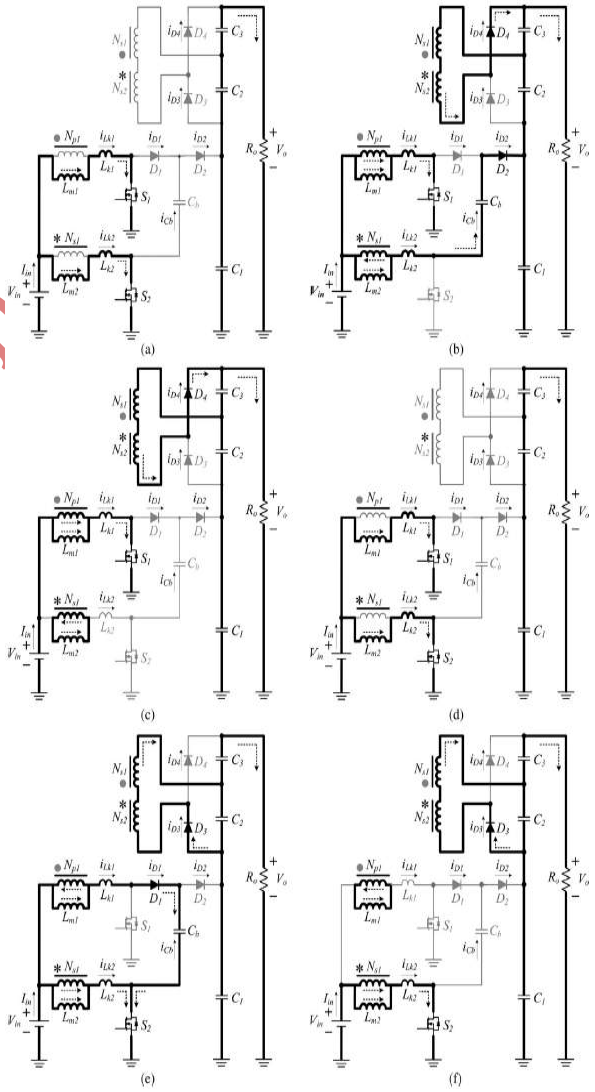

Fig. 5 Operating modes of the proposed converter. (a) Mode 1 [*t*0, *t*1]. (b) Mode 2 [*t*1, *t*2]. (c) Mode 3 [*t*2, *t*3]. (d) Mode 4 [*t*3, *t*4]. (e) Mode 5 [*t*4, *t*5]. (f) Mode 6 [*t*5, *t*0].

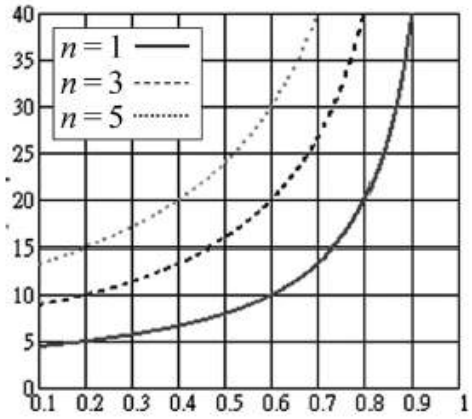

Fig.6 Voltage gain versus turns ratio *n* and duty cycle**.**

However the terms like Reverse-Recovery of diodes, Losses due to transformer switching, are not explained here. The performance for the inductors are disregarded because of the recycling of the energy. Fig. 8. Equivalent circuit including conduction losses of coupled inductors and semiconductor **components.** The equivalent circuit, which includes the conduction losses of coupled inductors and semiconductor components is shown in Fig.8, in which *rL*11 and *rL*21 are the copper resistances of primary windings of the coupled inductor; *rL*12 and *rL*22 are the copper resistances of secondary windings of the coupled inductor; *rDS*1 and *rDS*2 denote the on-resistance of power switches; *VD*1, *VD*2, *VD*3, and *VD*4 denote the forward biases of the diodes; and *rD*1, *rD*2, *rD*3, and *rD*4 are the resistances of the diodes.

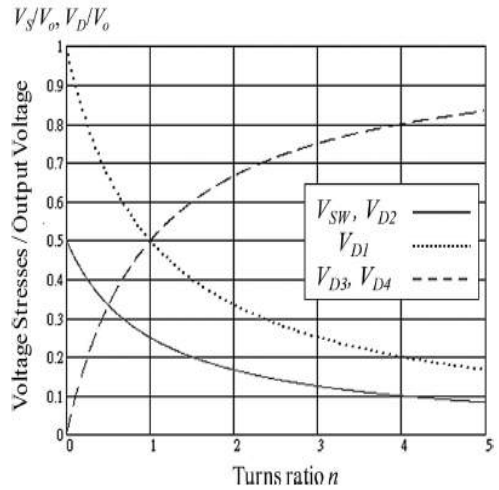

Fig.7.Voltage stresses on semiconductor components versus turns ratio *n*.

Small-ripple approximation was used to calculate conduction losses. Thus, all currents that pass through components were approximated by the dc components. The magnetizing currents and capacitor voltages are assumed constant because of

.

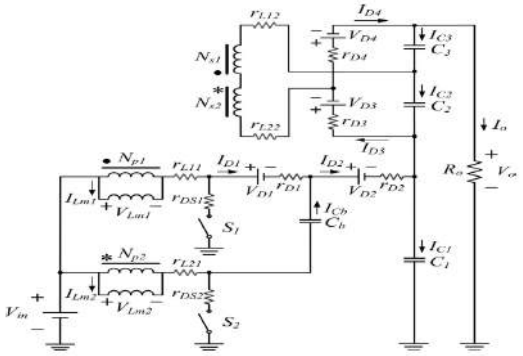

Fig. 8. Equivalent circuit including conduction losses of coupled inductors and semiconductor components.

the infinite values of magnetizing inductors and capacitors. Fig. 8 shows the PWM signals of *S*1 and *S*2.

The equivalent operating-states with4 modes, as shown.

Mode 1 [0, (D−0.5)]: Here the switches *S*1,*S*2 made ON, and *D*1-*D*2-*D*3- *D*4 are made OFF. The adopted , with the equation given by:

$$V_{\text{in}} = I_{Lm1}(r_{L11} + r_{DS1}) + V_{Lm1} \quad (14)$$

$$V_{\text{in}} = I_{Lm2}(r_{L21} + r_{DS2}) + V_{Lm2}. \quad (15)$$

Mode 2 [(D−0.5), 0.5]: Here, Switch *S*2 is made OFF, while *D*2 and*D*4 are made ON. The equiv. equation can be

$$V_{\text{in}} = (I_{Lm1} + nI_{D4}) \cdot (r_{L11} + r_{DS1}) + V_{Lm1} \quad (16)$$

$$V_{\text{in}} = (I_{Lm2} - nI_{D4}) \cdot (r_{L21} + r_{D2}) + V_{Lm2} + V_{D2} - V_{Cb} + V_{C1} \quad (17)$$

$$V_{C3} = n(V_{Lm1} - V_{Lm2}) - I_{D4}(r_{L21} + r_{L22} + r_{D4}) - V_{D4}. \quad (18)$$

Mode 3 [0.5, D]: This mode is similar to mode 1. The equivalent circuit in the figure10-c, and equation can be

$$V_{\text{in}} = I_{Lm1}(r_{L11} + r_{DS1}) + V_{Lm1} \quad (19)$$

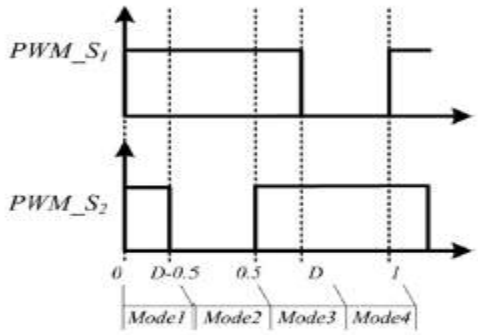

Fig.9. PWM signal of *S*1 and *S*2.

$$V_{\text{in}} = I_{Lm2}(r_{L21} + r_{DS2}) + V_{Lm2}. \tag{20}$$

Mode 4 [D, 1]: In this mode, power switch *S*1 is turned OFF, and diodes*D*1 and*D*3 are made On. The similar, with the below equation :

$$V_{\text{in}} = (I_{Lm2} + nI_{D3}) \cdot r_{L21} + V_{Lm2} + (I_{Lm1} + I_{Lm2}) \cdot r_{DS2} \tag{21}$$

$$V_{\text{in}} = (I_{Lm1} - nI_{D3}) \cdot (r_{L11} + r_{D1}) + V_{Lm1} + (I_{Lm1} + I_{Lm2}) \cdot r_{DS2} + V_{D1} + V_{Cb} \tag{22}$$

$$V_{C2} = n(V_{Lm2} - V_{Lm1}) - I_{D3}(r_{L21} + r_{L22} + r_{D3}) - V_{D3}. \tag{23}$$

The I_{avg} which goes across *D*1- *D2*, *D3*, and *D*4 can be derived by the capacitor charge balance.

In modes 1 and 3, both switches are turned OFF, and the average currents that pass through output filter Condensers *C*1-*C*2-*C*3

$$I_{C1} = I_{C2} = I_{C3} = -\frac{V_o}{R_o}. \tag{24}$$

In mode 2, the average currents that pass through output filter capacitors *C*1 and *C*3 are

$$I_{C1} = I_{D2} - \frac{V_o}{R_o} \tag{25}$$

$$I_{C3} = I_{D4} - \frac{V_o}{R_o}. \tag{26}$$

In mode 4, the average currents that pass through output filter capacitor *C*2 are as follows:

$$I_{C2} = I_{D3} - \frac{V_o}{R_o}. \tag{27}$$

On the basis of (33), we infer that the efficiency will be higher if the input voltage is considerably higher than the summation of the forward bias of the rectifiers. The evaluated Volte-Gain ann also the efficiency with different copper resistances and *rL*11 and *rL*21 are defined as *rL* . The other parameters in (33) are set as follows:

1) input voltage *V*in : 40 V;

2) Turns ratio *n* : 1;

3) load *Ro* : 200 Ω

4) on-resistances of switches *rDS*1 and *rDS*2 : 0.021 Ω;

5) Resistances of diodes *rD*1, *rD*2, *rD*3 , and *rD*4 : 0.01 Ω;

6) Forward bias of diodes *VD*1, *VD*2, *VD*3 , and *VD*4 : 1 V;

7) Copper resistances of secondary windings of coupled inductors *rL*12 and *rL*22=*rL* at a turns ratio *n* of 1.

Reveals that efficiency and voltage gain are affected by various coupled inductor winding resistors also the efficiency lowers to the extreme duty ratio.

D. Performance Comparison

For demonstrating the performance of the proposed converter, the proposed converter is compared with other high step-up interleaved converters introduced in [30] and [33] as shown Table I.

TABLE I: Converter Components and Parameters

Components	Symbols	Parameters
Magnetizing inductances	L_{m1}, L_{m2}	133µH
Leakage inductance	L_{k1}, L_{k2}	1.6H
Turns ratio	$N(N_s/N_p)$	1
Power switches	S_1, S_2	IRFP4227
Diodes	D_1, D_3, D_4 D_2	FCF06A-40 BYQ28E-200
Capacitors	C_b, C_2, C_3, C_1,	220 µf 470 µf

The high step-up interleaved converter introduced in [30] is also suitable as a candidate for high step-up, high-power conversion of the PV system, and the other high step-up interleaved converter introduced in [33], which is an asymmetrical interleaved structure as proposed converter is favorable for dc-micro grid applications.

IV.DESIGN OF THE PROPOSED CONVERTER

In control strategy, the proposed converter is as shown in Fig. 10. PV module and battery set are the main input power sources, which can be seen as an equivalent voltage source for the proposed converter, and the MPPT algorithm is employed by referring. Fig. 11 illustrates the measured waveforms of *Vgs*1, *Vgs*2, *iLk*1, *iLk*2, *Vds*1, *Vds*2 and *iLs* at *Po* = 1 kW. In Fig. 11(b), the switch voltage is clamped at 90 V, which is much smaller than the output voltage 380 V.

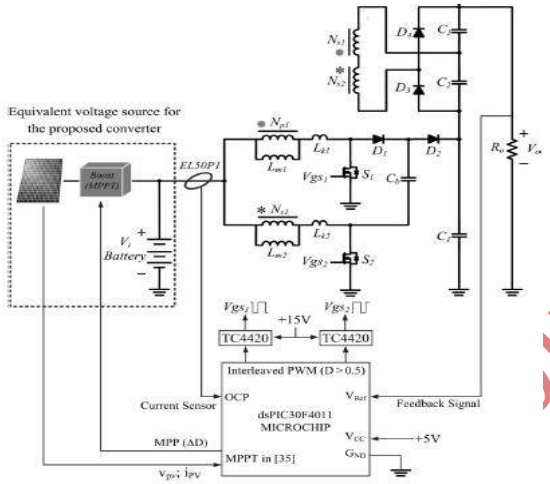

Fig. 10 Control strategy for the proposed converter.

Fig. 11(c) and Fig.11(d) illustrate the measured waveforms of *Vgs*1, *Vgs*2, *iD*1, *iD*2, *iD*3, and *iD*4 at *Po* = 1 kW. The measured waveforms are consistent with the steady-state analysis. Fig. 15 shows the simulation and experimental result of voltage on all capacitor to illustrate the high voltage storage and theoretical analysis. *VC*1 is equal to *VCb* plus output voltage of boost converter, and *VCb* is equal to the output voltage of the boost converter. Thus, *VC*1 is twice of *VCb*. *VC*2 is equal to *VC*3; both are nearly *VCb* because turns ratio *n* is set 1.The input current ripple *i*in and the currents *iLK*1 and *iLK*2 of the primary side of the coupled inductors at *Po* = 1 kW. The peak-to-peak current ripple is about 2A (6%), which confirms that the input current ripple is very low even if at high-power operation. The dynamic response due to the step load variation between 100 and 500W, and the output voltage is 380 V. Fig. 12 shows the measured efficiency of the proposed converter. The maximum efficiency is 96.8% at *Po* = 400W. At maximum output power, the conversion efficiency is about 96.1%.

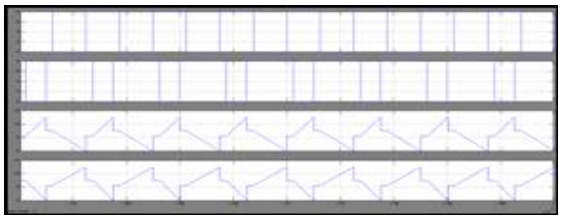

(a)and(b)

(c)

(d)

Fig. 11. Measured waveform at *Po* = 1 kW: (a) *Vg s*1, *Vg s*2, *iLk*1, and *iLk*2 . (b) *Vds*1, *Vds*2, and *iLs*. (c) *Vg s*1,*Vg s*2, *iD*1, and *iD*2. (d) *Vg s*1, *Vg s*2 , *iD*1, and *iD*2 .

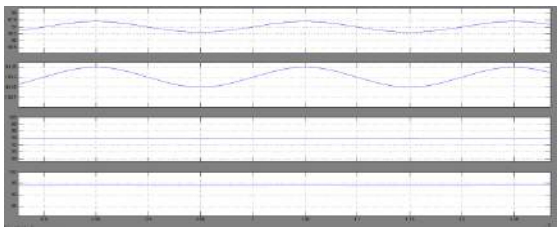

Fig.12. Simulation result of high-voltage storage of a capacitor.

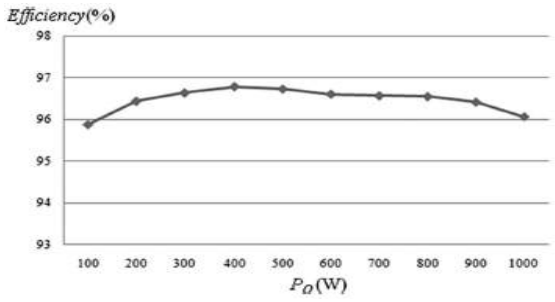

Fig. 13. Measured efficiency of the proposed converter.

V.CONCLUSION

This paper has presented the topological principles, steady state analysis, and experimental results for a our mentioned methodology. The presented technique for the converter design has been implemented successfully and in an efficiently high step-up conversion without an extreme duty ratio and a number of turns ratios through the voltage multiplier module and voltage clamp attribute. However the interleaved PWM technique decreases the currents that pass through each power switch and constrained the input current ripple by approximately 6%. These switches, conducted to low voltage rated and low on-state resistance MOSFET, can be selected. Furthermore, the full-load efficiency is 96.1% at *Po* = 1000 W, and the highest efficiency is 96.8% at *Po* = 400 W. Thus, the proposed converter is suitable for PV systems or other renewable energy applications that need high step-up high-power energy conversion.

VI. REFERENCES

[1] Y. Xiong, X. Cheng, Z. J. Shen, C. Mi, H.Wu, and V. K. Garg, "Prognostic and warning system for power-electronic modules in electric, hybrid electric, and fuel-cell vehicles," *IEEE Trans. Ind. Electron.*, vol. 55, no. 6, pp. 2268–2276, Jun. 2008.

[2] F. S. Pai, "An improved utility interface for micro-turbine generation system with stand-alone operation capabilities," *IEEE Trans. Ind. Electron.*, vol. 53, no. 5, pp. 1529–1537, Oct. 2006.

[3] H. Tao, J. L. Duarte, and M. A. M. Hendrix, "Line-interactive UPS using a fuel cell as the primary source," *IEEE Trans. Ind. Electron.*, vol. 55, no. 8, pp. 3012–3021, Aug. 2008.

[4] Z. Jiang and R. A. Dougal, "A compact digitally controlled fuel cell/battery hybrid power source," *IEEE Trans. Ind. Electron.*, vol. 53, no. 4, pp. 1094–1104, Jun. 2006.

[5] F. S. Pai, "An improved utility interface for micro-turbine generation system with stand-alone operation capabilities," IEEE Trans. Ind. Electron., vol. 53, no. 5, pp. 1529–1537, Oct. 2006.

[6] H. Tao, J. L. Duarte, and M. A. M. Hendrix, "Line-interactive UPS using a fuel cell as the primary source," IEEE Trans. Ind. Electron., vol. 55, no. 8, pp. 3012–3021, Aug. 2008.

[7] Z. Jiang and R. A. Dougal, "A compact digitally controlled fuel cell/battery hybrid power source," IEEE Trans. Ind. Electron., vol. 53, no. 4, pp. 1094–1104, Jun. 2006.